

## Vorticity dynamics during the start-up phase of gravity currents(\*)(\*\*)

C. HÄRTEL<sup>(1)</sup>, E. MEIBURG<sup>(2)</sup> and F. NECKER<sup>(1)</sup>

<sup>(1)</sup>*Institute of Fluid Dynamics, Swiss Federal Institute of Technology - Zürich, Switzerland*

<sup>(2)</sup>*Department of Aerospace Engineering, University of Southern California - Los Angeles, CA, USA*

(ricevuto il 18 Novembre 1998; approvato il 6 Maggio 1999)

**Summary.** — The flow during the start-up phase of two-dimensional gravity currents is investigated by numerical simulations. The focus of the study is on the dynamics of the initially vertical density interface which is deformed by the developing convective motion. Two different cases are considered, namely the lock-exchange flow and the release of a finite volume of dense fluid in deep surroundings. The viscous problem is addressed by direct numerical simulations based on the Boussinesq equations, which are integrated by high-order numerical schemes. The direct simulations are supplemented by vortex dynamics simulations using a vortex blob technique in order to study the underlying inviscid dynamics. Several distinct features of starting gravity currents are identified, among these the formation of start-up vortices very similar in nature to those observed for unstratified vortex sheets of finite extent. Moreover, the flow is shown to develop a pronounced Kelvin-Helmholtz-like instability at the interface, the details of which strongly depend on the ratio of buoyancy forces to viscous forces.

PACS 92.10.Ei – Coriolis effects.

PACS 47.55.Md – Stratified flows.

PACS 47.32.Cc – Vortex dynamics.

PACS 01.30.Cc – Conference proceedings.

### 1. – Introduction

Gravity or density currents are essentially horizontal flows of a denser fluid into a less dense fluid which are driven by gravitational forces. Gravity currents are commonly encountered in a variety of geophysical applications, well-known examples being moving atmospheric cold fronts, thunderstorm outflows, powder-snow avalanches or muddy underflows in lakes or oceans. Their study is also important in numerous engineering applications, for example in the context of industrial safety and

---

(\*) Paper presented at the International Workshop on “Vortex Dynamics in Geophysical Flows”, Castro Marina (LE), Italy, 22-26 June 1998.

(\*\*) The authors of this paper have agreed to not receive the proofs for correction.

environmental protection. A general discussion of their relevance in the natural and technical sciences can be found in [1-3].

In the laboratory, it is common to generate gravity currents by the sudden removal of a vertical splitter plate separating two fluids of different density in a channel [1, 4]. If the two fluid reservoirs are of equal height, the resulting current is usually termed a lock-exchange flow [1, 2], and is characterized by a pair of mutual intrusion fronts which travel along the bottom and the ceiling of the channel, respectively. Immediately upon the release, the flow passes through an initial transient during which the fluid is accelerated from rest and the frontal system forms. The duration of the initial transient is typically 5-10 time units  $\tilde{h}/\tilde{u}_b$  (a tilde designates a dimensional quantity here), where  $\tilde{h}$  and  $\tilde{u}_b$  are half the height of the channel and the buoyancy velocity, respectively [5]. In the subsequent fully developed flow the fronts propagate at a fairly constant speed.

Another extensively studied case is the release of a fixed volume of heavy fluid which is completely submerged in light fluid. We will refer to this case as a constant-volume release here; it features one intrusion front only, which is formed of heavy fluid and runs along the ground. Research on constant-volume releases has addressed both plane and radial spreadings, the latter having obvious applications to problems related to spillages of dense industrial gases or hydrocarbons on the sea [2]. Similar to lock-exchange flows, constant-volume releases also exhibit an initial transient during which the front is formed at the initially vertical interface at the leading edge. The transient is usually followed by a constant-speed phase which undergoes a transition to a self-similar state characterized by an ever decreasing speed of propagation [1, 2, 4].

While research has focused on the constant-speed phase and—for constant-volume releases—the self-similar phase, very little is known about the flow during the initial transient. Apart from the question of to what extent the initial transient will influence the later flow evolution, the start-up phase constitutes an interesting generic configuration in itself, which allows the study of stratified flows in situations where the density interface is aligned with the direction of gravitational acceleration. The experimental analysis of this flow is usually difficult due to the fact that the rapid removal of the separating splitter plate tends to create substantial disturbances at the leading edge. Theoretical difficulties originate in the genuinely unsteady and non-hydrostatic character of the initial flow. Consequently, shallow-water theory or steady-state balances which otherwise have been used successfully in the analysis of intrusion fronts [4, 6, 7], cannot be applied when it comes to investigating the initial phase of the flow evolution. So far, aspects of the start-up process have been addressed in a few computational studies only [8, 9].

The purpose of this paper is to study gravity currents in their initial transient by accurate numerical simulations. We will consider plane gravity currents both of the lock-exchange type and the finite-volume release kind. In particular, we will examine the early generation of vortical structures, which appear to play a crucial role in the subsequent interface dynamics. The dependence of the flow topology on the magnitude of the viscous forces will also be considered. Two different numerical approaches are employed, namely direct numerical simulations (DNS) and vortex dynamics simulations.

## 2. – Basic equations

In the present study, we deal exclusively with gravity currents driven by small density differences. Therefore, we employ the unsteady Boussinesq equations for the

mathematical description of the flow, in which variations in the density  $\tilde{\varrho}$  are generally neglected except for the buoyancy term. In dimensionless form the equations read

$$(1) \quad \frac{\partial u_k}{\partial x_k} = 0,$$

$$(2) \quad \frac{\partial u_i}{\partial t} + \frac{\partial(u_i u_k)}{\partial x_k} = -\frac{\partial p}{\partial x_i} + \frac{1}{\sqrt{Gr}} \frac{\partial^2 u_i}{\partial x_k \partial x_k} + \varrho e_i^g,$$

$$(3) \quad \frac{\partial \varrho}{\partial t} + \frac{\partial(\varrho u_k)}{\partial x_k} = \frac{1}{\sqrt{GrSc}^2} \frac{\partial^2 \varrho}{\partial x_k \partial x_k},$$

where  $u_i$  denotes the velocity vector,  $p$  the pressure, and  $\varrho$  the density.  $e_i^g$  is the unit vector in the direction of gravitational acceleration, which will always be aligned with  $x_3$  here, *i.e.*  $e_i^g = (0, 0, -1)^T$ . All terms in (1)-(3) have been made dimensionless by a characteristic vertical length scale  $\tilde{l}$ , the average density  $\tilde{\varrho}_a$ , and the buoyancy velocity  $\tilde{u}_b$

$$(4) \quad \tilde{u}_b = \sqrt{\tilde{g}' \tilde{l}}, \quad \text{where} \quad \tilde{g}' = \tilde{g} \frac{\Delta \tilde{\varrho}}{\tilde{\varrho}_a}.$$

In the above equations  $\tilde{g}'$  denotes the reduced gravity, and  $\Delta \tilde{\varrho} = \tilde{\varrho}_{\max} - \tilde{\varrho}_{\min}$  is the difference between the reservoir densities of light and heavy fluid. The dimensionless pressure  $p$  and density  $\varrho$  are given by

$$(5) \quad p = \frac{\tilde{p}}{\tilde{\varrho}_a \tilde{u}_b^2}, \quad \varrho = \frac{\tilde{\varrho} - \tilde{\varrho}_{\min}}{\Delta \tilde{\varrho}}.$$

Two dimensionless parameters arise from the normalization discussed above, namely the Grashof number  $Gr$ , which quantifies the ratio of buoyancy forces and viscous forces, and the Schmidt number  $Sc$ , which is the ratio of kinematic viscosity  $\tilde{\nu}$  and molecular diffusivity  $\tilde{K}$  in the density field,

$$(6) \quad Gr = \left( \frac{\tilde{u}_b \tilde{l}}{\tilde{\nu}} \right)^2, \quad Sc = \frac{\tilde{\nu}}{\tilde{K}}.$$

In order to assess the influence of viscous forces on the flow, we have varied the Grashof number in some of our direct simulations. The Schmidt number, on the other hand, was set to unity throughout.

For two-dimensional flows, which we will concentrate on here, the following transport equation for the vorticity  $\omega$  can be derived from (2):

$$(7) \quad \frac{D\omega}{Dt} \equiv \frac{\partial \omega}{\partial t} + u_k \frac{\partial \omega}{\partial x_k} = \frac{1}{\sqrt{Gr}} \frac{\partial^2 \omega}{\partial x_k \partial x_k} - \frac{\partial \varrho}{\partial x_1},$$

where  $D/Dt$  denotes the material derivative. The gravitational forcing is expressed by the second term on the right-hand side of (7), and it represents the baroclinic vorticity production which results in the accumulation of vorticity in the narrow region where the fluid density varies.

### 3. – Direct numerical simulations

In the direct simulations, the computational domain is a rectangular cavity of height  $2\tilde{h}$  and length  $L_1$ , which is filled with two fluids of different densities at rest. As the characteristic length scale  $\tilde{l}$  we employ the half-height  $\tilde{h}$  of the cavity. The initial set-up can be seen in the first graph of fig. 1, where, however, only a short section of the flow domain in  $x_1$  has been plotted. In our lock-exchange simulations  $L_1$  was generally much larger than the sections shown in the figures, in order to ensure that the boundaries at  $x_1 = \pm L_1/2$  have no effect on the flow in the region of interest, *i.e.* in the neighborhood of the interface. In the rectangular computational domain, the Boussinesq equations are solved in a vorticity-streamfunction formulation by a high-order numerical scheme, which employs a spatial discretization based on sine and cosine expansions in the longitudinal direction  $x_1$  together with high-order compact finite differences in  $x_3$ . The time discretization is performed in a fully explicit manner with a third-order-accurate low-storage Runge-Kutta scheme. A more detailed description of the numerical method can be found in [5, 10].

In fig. 1 the evolution of the density interface after the initial release is depicted for a Grashof number of  $Gr = 2 \cdot 10^9$ . Due to the production term in the vorticity budget (7), a vortex sheet is being generated at the location of the interface, the intensity of which grows with time. The early roll-up of the ends of this vortex sheet between times 1 and 2 is the most noticeable feature of the early flow evolution, and it is accompanied by increased local stretching rates. Due to its importance in aerodynamic applications, the roll-up phenomenon of finite length vortex sheets is a classical problem whose analysis dates back to the early theoretical work of Prandtl [11] and Kaden [12]. An overview over more recent theoretical progress can be found in [13]. However, even though recent careful and detailed experimental and computational results have been obtained, there are still a number of very fundamental unresolved issues regarding the principles that govern the formation and growth of such vortical structures [14-16]. Moreover, virtually all previous investigations apply to the case of constant density and nearly inviscid flow, while, to our knowledge, an in-depth analysis of finite vortex sheet dynamics in variable-density environments has not yet been performed.

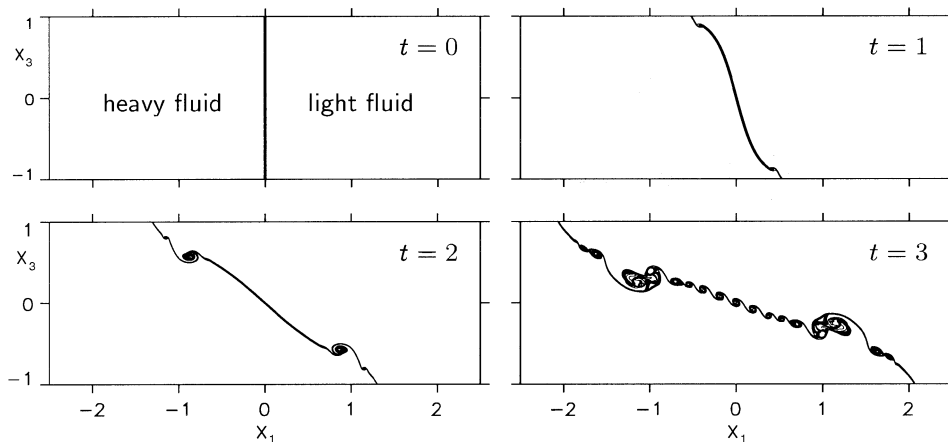


Fig. 1. – Lock-exchange flow at  $Gr = 2 \cdot 10^9$ , visualized by isocontours of density for various dimensionless times  $t$ . Simulation conducted with free-slip boundary conditions at  $x_3 = \pm 1$ .

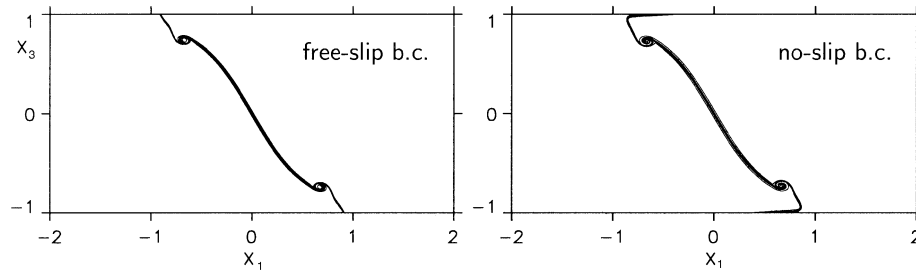


Fig. 2. – Isocontours of density for lock-exchange flows at time  $t = 1.5$ . Results for  $Gr = 2 \cdot 10^9$  and free-slip boundaries and no-slip boundaries at  $x_3 = \pm 1$ , respectively.

In the simulation shown in fig. 1 free-slip conditions were applied at the top and bottom boundaries, but we emphasize that the influence of the boundary conditions at  $x_3 = \pm 1$  on the flow evolution is marginal in the start-up phase. This is evidenced by fig. 2, in which flow fields at the same dimensionless time and for the same Grashof number are shown, but with different boundary conditions. For no-slip conditions (*i.e.* solid walls), thin boundary layers form, but they leave the flow structure in the interior of the flow domain virtually unaffected. The vortex sheet roll-up, as well as the tilting of the interface, proceed in essentially the same fashion in both cases.

The start-up vortices described above are clearly distinct from the Kelvin-Helmholtz vortices, which subsequently form as a result of an instability of the interface separating the two streams of different density. From fig. 1 it is seen that the Kelvin-Helmholtz-type instability occurs after the start-up vortices have formed, and that it results in a very regular pattern of small-scale vortices. While we found the initial roll-up process of the vortex sheet to be largely independent of the value of the Grashof number, the dynamics of the emerging interface instability is clearly a function of the ratio of viscous-to-buoyancy forces. The wavelength of the emerging vortices and their growth rate approximately scale with the thickness of the interface, which in turn

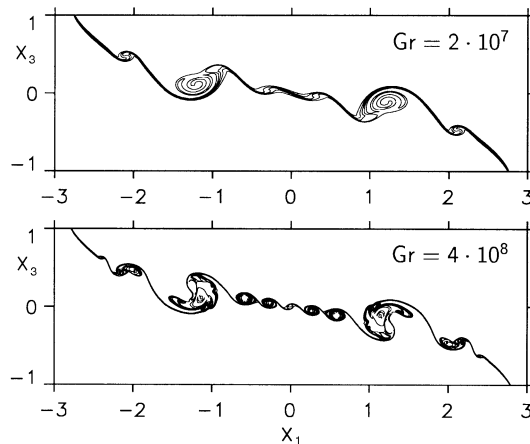


Fig. 3. – Isocontours of density for lock-exchange flows at time  $t = 4$ . Results for different Grashof numbers.

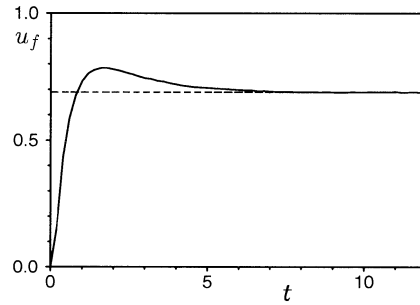


Fig. 4. – Front speed  $u_f$  as a function of time for  $\text{Gr} = 2 \cdot 10^9$  and free-slip boundary conditions at  $x_3 = \pm 1$ . The dashed line gives the asymptotic value that  $u_f$  approaches after the initial transient.

is determined by the value of the Grashof number. In fig. 3 results of lock-exchange flows at  $\text{Gr} = 2 \cdot 10^7$  and  $4 \cdot 10^8$ , respectively, are shown for the same dimensionless time  $t = 4$ . It is readily seen that the wavelength of the Kelvin-Helmholtz vortices decreases substantially with increasing Grashof number. During the later flow development, both Kelvin-Helmholtz vortices and start-up vortices undergo successive pairing events, which eventually lead to very large vortices in the interior of the channel [5].

The constant front speed of a developed lock-exchange flow in essence depends on the amount of circulation contained within the flow domain [5]. For free-slip boundaries and sufficiently high Grashof numbers the diffusion of vorticity across the boundaries becomes vanishingly small and all the circulation generated by the baroclinic production term remains within the flow domain. Therefore, the front speed becomes independent of Grashof number for about  $\text{Gr} > 10^8$  [5]. As an example, fig. 4 shows the time history of  $u_f$  for a lock-exchange flow at  $\text{Gr} = 2 \cdot 10^9$ . Starting from zero at  $t = 0$ ,  $u_f$  rapidly grows to a maximum at  $t \approx 1.5$  before it settles to a constant value of  $u_f = 0.69$  at the end of the initial transient (at  $t = 8$ , say). We have computed the integral mean of  $u_f$  over the initial transient and found it to be almost exactly equal to the asymptotic value of 0.69 of the fully developed flow. The constant-speed phase may be considered as an equilibrium state where the deposition of circulation at the continuously extending interface just balances the baroclinic production, but a non-equilibrium situation clearly prevails during the initial transient. Here circulation is already being generated at a constant rate, while the frontal system still needs to be accelerated from rest. In this stage the circulation produced is mainly stored in the developing start-up vortices which afterwards accelerate the fronts during the further flow evolution. This then leads to the overshoot of  $u_f$  observed in fig. 4.

Similar to lock-exchange flows, finite-volume releases also exhibit the formation of a pair of start-up vortices at that portion of the interface which initially is vertical. The formation of these start-up vortices can be seen in fig. 5 where results are shown from a simulation of the release of an originally rectangular patch of heavy fluid embedded in a second fluid of smaller density. The initial height of the patch of heavy fluid is equal to half the channel height, meaning that the dynamics of this flow may somewhat differ from finite-volume releases in very deep surroundings (which often are of more interest in practice). However, a comparison of fig. 5 with results to be presented in the subsequent section reveals that the influence of the finite height of the channel is

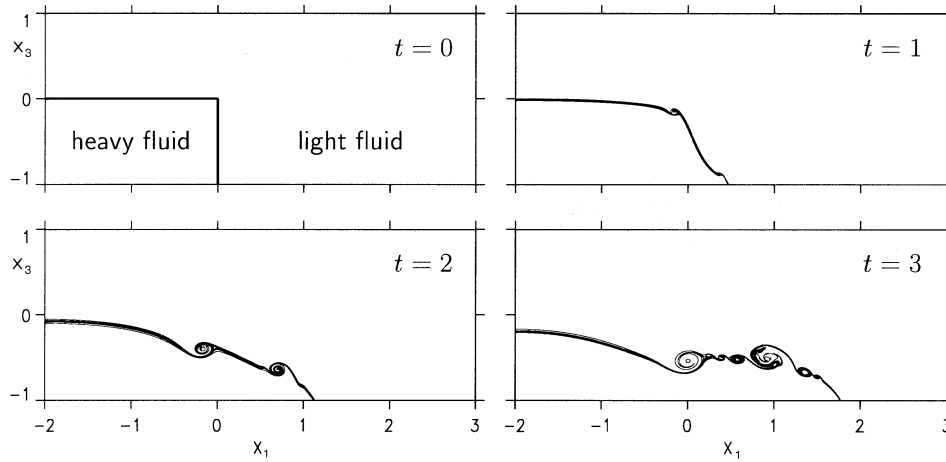


Fig. 5. – Time evolution of a constant-volume release at  $Gr = 10^9$ , visualized by isocontours of density.

marginal in the present case. From fig. 5 it is seen that, like in the lock-exchange case shown in fig. 1, the formation of two early start-up vortices is followed by a Kelvin-Helmholtz instability of the central interfacial segment, which sets in between times 2 and 3. Due to the mass transport associated with the developing front, the height of the pool of dense fluid is constantly decreasing with time. Also, the originally horizontal part of the interface becomes curved. It is interesting to note that this curved part still does not display any indication of an instability, even at the fairly late time of  $t = 3$ , although the resulting horizontal density gradients give rise to a substantial production of vorticity along the entire interface. Furthermore, there is no indication that any of the downstream vortical structures will migrate upstream past the initial front location. Consequently, a major portion of the interface remains smooth and does not contribute to the entrainment of lighter fluid. A more detailed investigation of this aspect is currently under way.

#### 4. – Vortex dynamics simulations

The case of inviscid dynamics can be analyzed particularly efficiently by means of Lagrangian vortex dynamics simulations. In the following, these are based on the vorticity equation (7) where the first term on the right-hand side, representing viscous diffusion, is neglected. In the absence of diffusion, vorticity will thus remain confined to the interface for all times, and the governing equation for the evolution of the local circulation strength  $\gamma$  along the interface takes the form

$$(8) \quad \frac{D\gamma}{Dt} = \frac{\partial x_3}{\partial s},$$

where  $s$  denotes the arclength along the interface [17]. In our simulations we discretize the vorticity field into finite-size vortex blobs with a Gaussian distribution function [18]. Since the simulations typically involve no more than  $O(10^3)$  of these elements, the blob

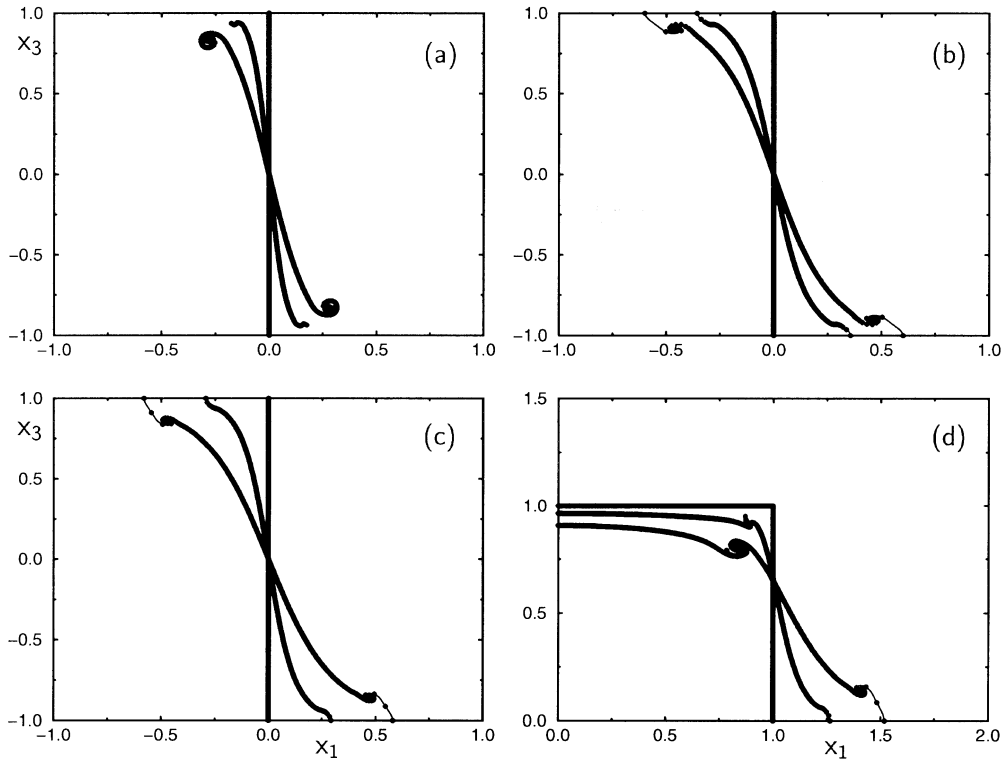


Fig. 6. – Several model problems investigated by inviscid vortex dynamics simulations. (a) A vortex sheet of finite extent and with constant circulation production in an infinite fluid domain. The roll-up of the vortex sheet ends, as well as the overall rotation of the sheet, are shown for times 0.01, 0.7, and 1.1. (b) The effect of the presence of horizontal walls on the evolution of the sheet. Times shown are 0.01, 1.1, and 1.5. The roll-up is somewhat delayed by the walls. (c) The vortex sheet evolution at the same times as in (a), if the circulation production is governed by the Boussinesq approximation to the equations of motion. (d) The evolution of an initially rectangular patch of heavy fluid submerged in an infinite domain of lighter fluid. Times are 0.01, 0.7, and 1.1. Strong start-up vortices form at both ends of the vertical portion of the interface.

velocities can efficiently be obtained from the Biot-Savart law by means of direct summation. The blobs have a core radius of 0.02 and are initially spaced one quarter of a core radius apart. Periodic remeshing adds additional blobs in those regions where interfacial length is being generated, in order to maintain an adequate discretization. A second-order explicit predictor-corrector method with automatic error control is employed to advance the simulations in time.

Some elementary aspects of the evolution of a finite length vortex sheet are demonstrated by the model problem depicted in fig. 6(a). The vortex sheet, embedded in a domain of infinite size (*i.e.* without boundaries), initially is oriented along the vertical direction, and at time  $t = 0$  it extends from  $x_3 = -1$  to  $x_3 = 1$ . For simplicity, the initial rate of circulation production is maintained throughout the calculation, even as the local orientation of the sheet varies with time. Indicated by a solid line are the instantaneous shapes of the vortex sheet at times 0.01, 0.7, and 1.1 (the respective solid

lines are better visible in graphs (b)-(d) of fig. 6). The dots indicate the instantaneous locations of the *initially present* vortex blobs, thereby providing information on the time integral of the rate at which local interfacial length has been generated, *i.e.* at which the interface has been stretched. The rapid roll-up of the vortex sheet ends and the overall rotation of the entire sheet are clearly visible and bear striking similarity with the evolution of the interface seen in fig. 1.

Figure 6(b) demonstrates the modification caused to the vortex sheet evolution by horizontal walls located at  $x_3 = -1$  and  $x_3 = 1$ , with all other parameters held constant. The times shown are 0.01, 1.1, and 1.5. The figure indicates that the intense roll-up process still occurs, but that it is somewhat delayed by the presence of the walls. Little stretching of the vortex sheet occurs in the interior of the flow domain, but the distribution of the initially present vortex blobs in the immediate vicinity of the walls indicates that a substantial amount of interfacial length has been generated in this flow region.

Finally, fig. 6(c) shows the interfacial evolution for the full time-dependent and locally varying circulation production according to the equation provided above, at the same times as those shown in fig. 6(a). A comparison of figs. 6(b) and (c) indicates that, at least at these early times, temporal changes in the local circulation production rate are of limited importance. The emergence of the start-up vortex is still essentially due to the roll-up of the vortex sheet end, and interfacial length is generated to allow the rolled up portion of the interface to remain connected to the wall.

The corresponding situation in an infinitely deep reservoir (fig. 6(d)) shows similarities as well as differences. It should be pointed out that a vortex dynamics approach is particularly suitable for simulating the evolution in a reservoir of infinite extent, since only the interface needs to be represented computationally. In fig. 6(d), the spreading of a rectangular patch of heavy fluid is shown at times 0.01, 0.7, and 1.1. The circulation production initially is most intense along the vertical segment of the interface, while its horizontal counterpart remains nearly passive for early times. As a result, the upper end of the vertical interface rolls up in a fashion that is quite similar to fig. 6(a). The lower segments of the vertical interface, on the other hand, behave quite

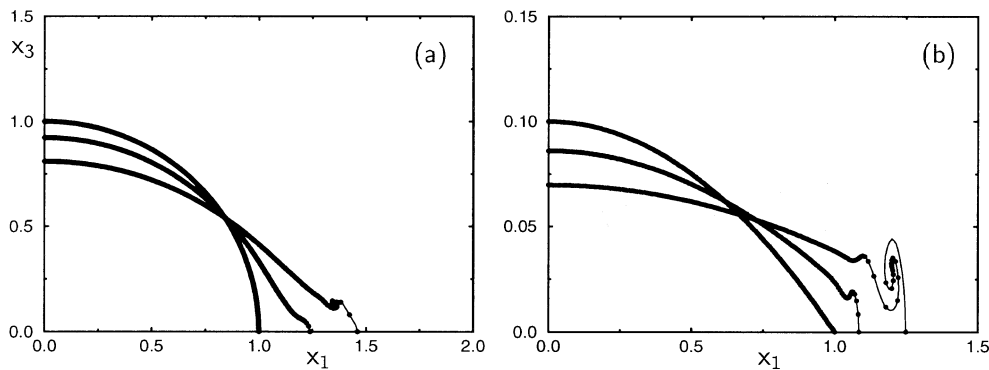


Fig. 7. – (a) Spreading of an initially semi-circular patch of heavy fluid in an infinite domain, shown at times 0.01, 0.7, and 1.1. The nature of the start-up vortex near the lower wall remain largely unaffected by the global shape of the interface. (b) The spreading of an initially shallow patch of heavy fluid in an infinite domain, shown at times 0.01, 1.5, and 2.5. Even this shallow patch of heavy fluid results in the formation of a strong start-up vortex.

similarly to the lock-exchange case of fig. 6(c). The results obtained by [9] for the radially symmetric case show strong qualitative similarities, even for density ratios that lie beyond the regime of validity of the Boussinesq approximation.

Figure 7(a) demonstrates that a fluid patch bounded by an initially circular interface gives rise to a rolled up vortex only near the lower wall. Its size and shape, shown for times 0.01, 0.7, and 1.1, evolve in a fashion that is nearly identical to the cases shown in figs. 6(c) and (d), which suggests that the dynamics of the start-up vortex near the lower horizontal wall are dominated by *local* effects. Finally, fig. 7(b) shows the evolution of a much shallower patch of heavy fluid, initially bounded again by an interface in the shape of a circular segment, at times 0.01, 1.5, and 2.5 (note the different scale on the  $x_3$ -axis in fig. 7(a) and (b)). It is interesting to note that even this shallow fluid patch results in a strong start-up vortex, although at a somewhat later time.

## 5. – Conclusions

Direct numerical simulations and vortex dynamics simulations of lock-exchange flows and finite-volume releases in deep surroundings were conducted. The computational results indicate that the initial, transient phase of gravity currents gives rise to several interesting phenomena. For both types of flows the early evolution is governed by the emergence of intense start-up vortices which are very similar in nature to those observed for unstratified vortex sheets of finite extent. The structure of these start-up vortices was found to depend only weakly on the Grashof number. This is in contrast to the dynamics of the subsequently evolving smaller-scale vortices at the interface which appear to be triggered by a Kelvin-Helmholtz-like instability. It was shown that the wavelength of these vortices substantially decreases with increasing Grashof number. Extensions to Boussinesq flows of the considerable analytical body of work available for the roll-up process of vortex sheets in constant density flows should be able to contribute significantly to a better understanding of the dynamics that govern the generation and evolution of the pronounced start-up vortices described here.

\* \* \*

The authors wish to thank Prof. L. KLEISER for a stimulating discussion that initiated the present research. Part of the work was conducted while EM was a guest at the Institute of Fluid Dynamics at ETH Zürich.

## REFERENCES

- [1] SIMPSON J. E., *Gravity Currents: in the Environment and the Laboratory*, 2nd edition (Cambridge University Press, Cambridge) 1997.
- [2] FANNELØP T. K., *Fluid Mechanics for Industrial Safety and Environmental Protection* (Elsevier, Amsterdam) 1994.
- [3] HUPPERT H. E., *J. Fluid Mech.*, **173** (1986) 557.
- [4] ROTTMAN J. W. and SIMPSON J. E., *J. Fluid Mech.*, **135** (1983) 95.
- [5] HÄRTEL C., MEIBURG E. and NECKER F., submitted to *J. Fluid Mech.* (1998).
- [6] BENJAMIN T. B., *J. Fluid Mech.*, **31** (1968) 209.
- [7] KLEMP J. B., ROTUNNO R. and SKAMAROCK W. C., *J. Fluid Mech.*, **269** (1994) 169.
- [8] DALY B. J. and PRACHT W. E., *Phys. Fluids*, **11** (1968) 15.

- [9] ZHANG X. J. and GHONIEM A. F., *Transport Element Method for Axisymmetric Variable-Density Flow and its Application to the Spread and Dispersion of a Dense Cloud*, in *Vortex Flows and Related Numerical methods II, ESAIM Proc.*, edited by Y. GAGNON *et al.* (SMAI, Paris) 1996.
- [10] HÄRTEL C., KLEISER L., MICHAUD M. and STEIN C. F., *J. Engin. Math.*, **32** (1997) 103.
- [11] PRANDTL L., *Über die Entstehung von Wirbeln in der idealen Flüssigkeit, mit Anwendung auf die Tragflügeltheorie und andere Aufgaben*, in *Vorträge aus dem Gebiete der Hydro- und Aerodynamik, Innsbruck 1922*, edited by TH. V. KÁRMÁN and T. LEVI-CIVITA (Springer, Berlin) 1924.
- [12] KADEN H., *Ing. Arch.*, **2** (1931) 140.
- [13] SAFFMAN P. G., *Vortex Dynamics* (Cambridge University Press, Cambridge) 1992.
- [14] DIDDEN N., *Z. Angew. Math. Phys.*, **30** (1979) 101.
- [15] AUERBACH D., *J. Fluid Mech.*, **183** (1987) 185.
- [16] NITSCHKE M. and KRASNY R., *J. Fluid Mech.*, **276** (1994) 139.
- [17] BAKER G. R., MEIRON D. I. and ORSZAG S. A., *Phys. Fluids*, **23** (1980) 1485.
- [18] LEONARD A., *J. Comput. Phys.*, **37** (1980) 289.